

# Radiofrequency Ablation, MR Thermometry, and High-Spatial-Resolution MR Parametric Imaging with a Single, Minimally Invasive Device<sup>1</sup>

M. Arcan Ertürk, PhD<sup>2</sup>  
 Shashank Sathyanarayana Hegde, PhD<sup>3</sup>  
 Paul A. Bottomley, PhD

## Purpose:

To develop and demonstrate in vitro and in vivo a single interventional magnetic resonance (MR)-active device that integrates the functions of precise identification of a tissue site with the delivery of radiofrequency (RF) energy for ablation, high-spatial-resolution thermal mapping to monitor thermal dose, and quantitative MR imaging relaxometry to document ablation-induced tissue changes for characterizing ablated tissue.

## Materials and Methods:

All animal studies were approved by the institutional animal care and use committee. A loopless MR imaging antenna composed of a tuned microcable either 0.8 or 2.2 mm in diameter with an extended central conductor was switched between a 3-T MR imaging unit and an RF power source to monitor and perform RF ablation in bovine muscle and human artery samples in vitro and in rabbits in vivo. High-spatial-resolution (250–300- $\mu\text{m}$ ) proton resonance frequency shift MR thermometry was interleaved with ablations. Quantitative spin-lattice (T1) and spin-spin (T2) relaxation time MR imaging mapping was performed before and after ablation. These maps were compared with findings from gross tissue examination of the region of ablated tissue after MR imaging.

## Results:

High-spatial-resolution MR imaging afforded temperature mapping in less than 8 seconds for monitoring ablation temperatures in excess of 85°C delivered by the same device. This produced irreversible thermal injury and necrosis. Quantitative MR imaging relaxation time maps demonstrated up to a twofold variation in mean regional T1 and T2 after ablation versus before ablation.

## Conclusion:

A simple, integrated, minimally invasive interventional probe that provides image-guided therapy delivery, thermal mapping of dose, and detection of ablation-associated MR imaging parametric changes was developed and demonstrated. With this single-device approach, coupling-related safety concerns associated with multiple conductor approaches were avoided.

©RSNA, 2016

*Online supplemental material is available for this article.*

<sup>1</sup>From the Department of Radiology, Johns Hopkins University, 600 N Wolfe St, Park 310, Baltimore, MD 21287. Received July 1, 2015; revision requested September 4; revision received February 15, 2016; accepted March 24; final version accepted March 30. **Address correspondence to** P.A.B. (e-mail: [bottoml@mri.jhu.edu](mailto:bottoml@mri.jhu.edu)).

## Current addresses:

<sup>2</sup>Center for Magnetic Resonance Research, University of Minnesota Medical School, Minneapolis, Minn.

<sup>3</sup>Philips Innovation Campus, Philips Healthcare, Bangalore, India.

Supported by the National Institutes of Health (R01 EB007829).

M.A.E. and S.S.H. contributed equally to this work.

©RSNA, 2016

**M**agnetic resonance (MR) imaging-guided radiofrequency (RF) ablation studies have previously involved the use of (a) dedicated ablation catheters for delivering RF energy while monitoring treatment via relaxation time-based MR image contrast changes (1) or (b) MR thermometry (2–4) performed with separate MR imaging detectors. In a safe ablation procedure, hazardous coupling to the RF applicator and/or cables needs to be avoided during MR imaging. Furthermore, the procedure requires fast high-spatial-resolution imaging to locate the applicator, demarcate the target tissue, and monitor the energy delivery, as well as monitor the tissue response at a sufficiently high spatial resolution to minimize potential collateral damage. The introduction of intravascular MR imaging probes at magnetic field strengths of 3 T and higher affords 80–300- $\mu$ m transluminal resolution at speeds of up to several frames per second (5–8). Until now, the use of these probes was primarily limited to imaging. An earlier

application to provide imaging guidance and thermally enhance gene therapy delivery at 1.5 T was limited in resolution by the available signal-to-noise ratio and did not include spin-lattice (T1) and spin-spin (T2) relaxation time mapping of the acute tissue response (9,10).

Here, we tested whether a single, loopless, 3-T MR imaging antenna (5,11) could be used interchangeably to (a) image a target site prior to RF ablation, (b) deliver RF energy for ablation, (c) monitor local temperature change by using high-spatial-resolution MR thermometry, and (d) confirm tissue damage after ablation with high-spatial-resolution relaxation-weighted and quantitative T1 and T2 mapping (12–14). The purpose was to develop and demonstrate in vitro and in vivo that a single interventional MR device could be used to integrate the functions of precise identification of a tissue site with the delivery of RF energy for ablation, high-spatial-resolution thermal mapping to monitor thermal dose, and quantitative MR imaging relaxometry to document ablation-induced tissue changes for characterization of ablated tissue.

MHz (dielectric constant, 63.5; electrical conductivity, 0.72 siemen/m). The temperature distribution induced by the electrical field around the probe was calculated from the Pennes heat transfer equation (specific heat, 3421 J/kg/K; thermal conductivity, 0.49 W/m/K) by using Semcad software (Schmid & Partner Engineering) with a baseline temperature of 37°C and excitations of 30, 60, and 120 seconds at RF power levels of 10, 20, 30, and 60 W during ablation. Temperature was computed for 300 seconds, starting with each ablation. Thermal dosage was assessed from the maximum absolute temperature and the cumulative equivalent minutes at 43°C (CEM<sub>43</sub>), a metric commonly used to assess thermal exposure during ablation (15). A CEM<sub>43</sub> of more than 80 minutes can cause tissue damage in human muscle (16), while necrosis generally ensues at CEM<sub>43</sub> of more than 340 minutes (17,18). Tissue volumes with temperatures of at least 42°C, 47°C, and 60°C and with a CEM<sub>43</sub> of 80 and 340 minutes were used to predict ablated tissue volumes (16,18).

### Advances in Knowledge

- A single, multifunctional, interventional MR imaging device was developed for image-guided localized radiofrequency (RF) ablations, monitoring of thermal dose by using high-spatial-resolution (0.3 × 0.3-mm in-plane resolution) thermal mapping, and documenting ablation-induced parametric tissue changes with quantitative MR imaging.
- High-spatial-resolution (approximately 300- $\mu$ m) 3-T MR imaging afforded temperature mapping in less than 8 seconds and was used to monitor ablation temperatures in excess of 85°C delivered by the same interventional MR imaging device in tissue specimens in vitro and in vivo in a rabbit model.
- Quantitative parametric maps demonstrated up to a twofold variation in mean MR imaging relaxation times after ablation versus before ablation.

### Materials and Methods

#### Electromagnetic and Thermal Simulations

The loopless antenna used in our study is an interventional MR imaging probe fabricated from a miniature coaxial cable terminated with an extended inner conductor that forms a “whip” for RF transmission and reception (9). A full-wave electromagnetic field analysis (Semcad X; Schmid & Partner Engineering, Zürich, Switzerland) was used (M.A.E., with 5 years of experience in electromagnetic simulations) to compute the electrical fields generated by the probe inside a homogeneous cylindrical phantom of human muscle at 128



### Implication for Patient Care

- A single 3-T MR imaging antenna can be used for high-spatial-resolution image-guided RF ablation, MR imaging thermometry, and characterization of tissue response.

### Hardware and MR Imaging Acquisition

Experiments were conducted with a 3.0-T whole-body Achieva MR System (Philips Medical Systems, Best, Netherlands). In vitro and percutaneous in vivo studies involved the use of a loopless antenna constructed with a

#### Published online before print

10.1148/radiol.2016151447 Content codes:  

Radiology 2016; 281:927–932

#### Abbreviations:

CEM<sub>43</sub> = cumulative equivalent minutes at 43°C  
RF = radiofrequency

#### Author contributions:

Guarantors of integrity of entire study, all authors; study concepts/study design or data acquisition or data analysis/interpretation, all authors; manuscript drafting or manuscript revision for important intellectual content, all authors; approval of final version of submitted manuscript, all authors; agrees to ensure any questions related to the work are appropriately resolved, all authors; literature research, all authors; experimental studies, all authors; and manuscript editing, all authors

Conflicts of interest are listed at the end of this article.

400-mm-long semirigid copper coaxial cable (UT-85-C; Microcoax, Pottstown, Pa) with an outer diameter of 2.2 mm and a 39-mm-long whip (S.S.H., with 11 years of experience with probes). In vivo intravascular studies involved the use of a biocompatible loopless antenna made from a nitinol hypotube with an 0.8-mm outer diameter, with a 42-mm-long whip (M.A.E., S.S.H., and P.A.B. [who had 21 years of experience with such probes]), as pictured in Figure E1a (online) (5). A nonmagnetic RF switch connected the probe to either (a) the MR imaging unit via a tuning-matching box during MR imaging acquisition (5) or (b) an RF power amplifier (BT00250-Gamma-CW; Tomco Technologies, Stepney, Australia) (Fig E1b [online]). The power amplifier was driven by a frequency synthesizer (PTS 160; Programmed Test Source, Littleton, Mass) for performing ablations in the imaging unit (switching time, 3–5 seconds), and the ablation power (128 MHz, 30–60 W) was monitored (LB 480A; Ladybug Technologies, Santa Rosa, Calif) at the amplifier output.

For MR imaging performed to localize the probe relative to the ablation target and monitor probe ingress and quantitative T1 and T2 mapping, gradient-echo sequences, turbo spin-echo sequences, and the “MIX” sequence (a combination of inversion-recovery imaging and turbo spin-echo imaging, Philips Medical Systems; M.A.E., S.S.H.) were used. The vendor’s analysis tools were used to compute T1 and T2 maps (19). MR imaging thermometry was performed by using the proton resonance frequency shift method (20). A temperature coefficient of  $-0.01$  parts per million per degree Celsius was used to convert thermometric phase images acquired by the probe to temperature maps (20,21). Large temperature changes near the probe that caused “phase wraps” were unwrapped in the image field of view, starting furthest (ie, coolest) from the probe, where phase wraps were minimal, and proceeding toward the probe (S.S.H.). Multiple phase wraps at distances of less than 5 mm from the probe confounded the unwrapping algorithm and were color masked in the displayed results.

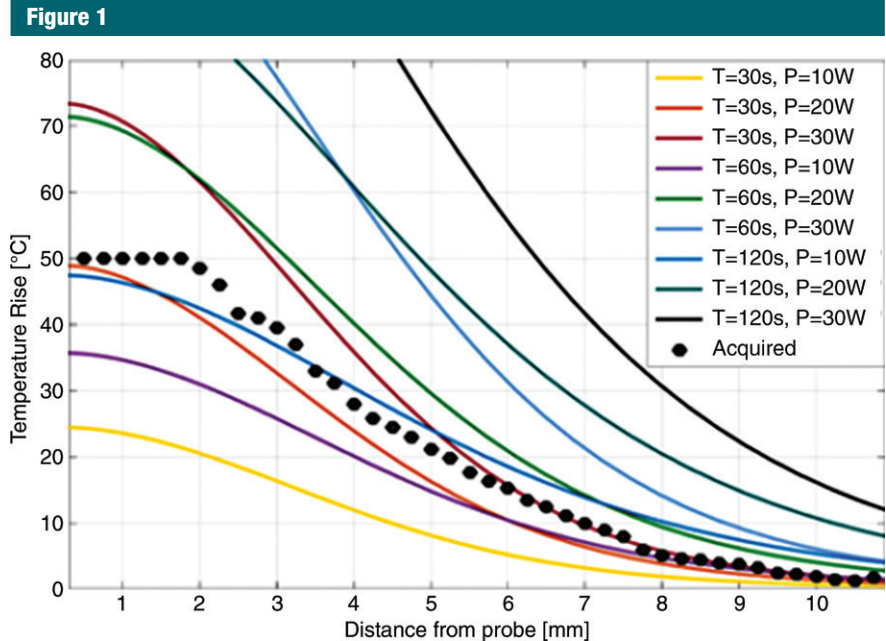


**Figure 1:** Graph shows computed temperature increase profiles 20 seconds after termination of ablation at various power ( $P$ ) levels in watts versus radial distance from the probe (solid lines). Experimental MR imaging thermometry data acquired from bovine muscle tissue with power of 30 W and time ( $T$ ) of 120 seconds are plotted as points (also see Fig 2).

MR thermometry data were compared with the numerical analysis as a function of radial distance from the cable-whip junction of the probe (M.A.E., S.S.H.). The preablation temperature of the saline bath used for in vitro studies was  $25^{\circ}\text{C}$ , and a preablation temperature of  $35^{\circ}\text{C}$  was assumed for the healthy rabbit in vivo. These baseline temperatures were added to the temperature change detected with proton resonance frequency thermometry for reporting final temperatures.

#### In Vitro and in Vivo Experiments

In vitro experiments were performed with the semirigid probe inserted directly into bovine muscle specimens and in the lumens of porcine aortas immersed in a 3.5-g/L saline bath (M.A.E., S.S.H.). In vivo studies were approved by our institutional animal care and use committee. Two New Zealand White rabbits were sedated with intramuscular acepromazine (1 mg per kilogram of body weight) and ketamine (40 mg per kilogram of body weight), induced with intravenous sodium thiopental, and

intubated to maintain an open airway (S.S.H.). In one in vivo protocol, the semirigid probe was inserted into the thigh via percutaneous puncture. In another, the biocompatible probe was advanced into the descending aorta to the renal bifurcation (with vessel sizes comparable to those of human coronary or renal arteries) via a femoral incision by using contrast material-enhanced computed tomography. The specimens were then transferred to the MR imaging unit. The three-point planning tool on the imaging unit was used to prescribe a plane that contained a substantial portion of the probe. Postmortem, the vessel section ablated by the probe was assessed for ablation injury and discoloration by means of gross examination.

## Results

### Electromagnetic and Thermal Response Simulations

The numerically computed temperature distribution 60 seconds after commencing ablation at 20-W power is

**Calculated Tissue Volumes with Maximum Temperature Higher Than 42°C, 47°C, and 60°C and with CEM<sub>43</sub> Values More Than 80 and 340 Minutes Used to Predict Ablated Tissue Volumes**

Ablation Duration and Power	Tissue Volume at Maximum Temperature Higher Than 42°C (cm <sup>3</sup> )	Tissue Volume at Maximum Temperature Higher Than 47°C (cm <sup>3</sup> )	Tissue Volume at Maximum Temperature Higher Than 60°C (cm <sup>3</sup> )	Tissue Volume at CEM <sub>43</sub> Duration More Than 80 Min (cm <sup>3</sup> )	Tissue Volume at CEM <sub>43</sub> Duration More Than 340 Min (cm <sup>3</sup> )
<b>30 sec</b>					
10 W	3.5	1.4	0.4	0.8	0.7
20 W	8.0	3.5	1.2	2.5	2.0
30 W	12.5	5.8	2.0	4.3	3.5
60 W	26.1	12.5	4.9	10.7	8.6
<b>60 sec</b>					
10 W	7.7	3.2	0.8	2.2	1.7
20 W	16.9	7.7	2.6	6.1	4.8
30 W	26.0	12.3	4.6	10.5	8.4
60 W	49.0	26.0	10.5	23.0	19.1
<b>120 sec</b>					
10 W	16.5	7.1	1.9	5.5	4.2
20 W	33.8	16.5	5.8	14.2	11.4
30 W	47.0	25.7	10.0	22.0	18.4
60 W	73.0	47.0	22.1	39.8	35.0

Note.—According to references 16 and 18.

shown in Figure E2a and E2b (online). The temperature increase profiles on an axial section centered at the probe cable- whip junction 20 seconds after ablation for 30-, 60-, and 120-second-long ablations at 10, 20, and 30 W of power are plotted in Figure 1. The ablated area can be enlarged by increasing either the ablation time (eg, yellow line vs purple line, Fig 1) or the power level (eg, yellow line vs brown line, Fig 1). The Table lists the volumes of tissue with temperatures of at least 42°C, 47°C, and 60°C and with CEM<sub>43</sub> of at least 80 and 340 minutes. The experimentally measured temperature increase profile in bovine tissue after a 30-W, 120-second-long ablation (black points on Fig 1) is consistent with the computed temperature profile from the 120-second-long ablation at 10 W after accounting for the cable and hardware losses (22).

**In Vitro and in Vivo Experiments**

The preablation MR images obtained in bovine muscle by using the semirigid probe appeared largely uniform (Fig E3a [online]). Ablation produced temperatures that exceeded 75°C, as measured

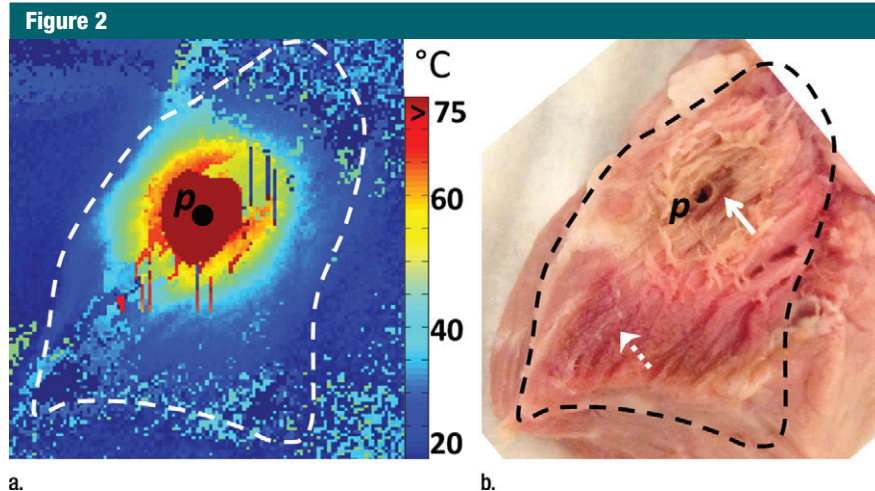


**Figure 2:** (a) MR thermometry image shows the temperature distribution during ablation (power of 30 W and time of 120 seconds). The dark red mask around the probe corresponds to areas with temperatures above 75°C. (b) Gross photograph shows that brown discoloration of the lesion is evident after ablation (solid arrow), while unaffected tissue remains pinkish (dashed arrow). Slight changes in the shape of the tissue before and after ablation are caused by the effects of ablation and saline immersion. *p* = probe.

with MR thermometry (Fig 2a). The measured size of the ablated volume (temperature change > 50°C) was 1.5 cm<sup>3</sup>. After ablation, the high-spatial-resolution MR images showed hypointensity (Fig E3b [online]) in the ablated region, which was verified at gross

examination after MR imaging (Fig 2b). Pre- and postablation T1 maps (Fig E3c and E3d [online], respectively) and pre- and postablation T2 maps (Fig E3e and E3f [online], respectively) show regions of heterogeneity at the ablation site (annotated ellipses), wherein T1



is halved (mean  $\pm$  standard deviation, 320 msec  $\pm$  91 vs 182 msec  $\pm$  72, respectively, for Fig E3d vs Fig E3c [online]) and T2 is doubled (96 msec  $\pm$  15 vs 197 msec  $\pm$  49, respectively, for Fig E3f vs Fig E3e [online]).

With the semirigid probe in a porcine aorta, preablation MR images obtained with 150- $\mu$ m in-plane resolution depict a well-defined vessel wall (Fig 3a). High-spatial-resolution (250- $\mu$ m) MR thermometry images show delivery of a 12°C thermal dose immediately above the probe (highlighted area on Fig 3b). MR images obtained inside a rabbit aorta in vivo by using the biocompatible nitinol probe similarly demonstrated the vessel wall and the surrounding tissue (Fig E4a [online]). High-spatial-resolution MR imaging thermometry (with 300- $\mu$ m in-plane resolution) showed delivery of a thermal dose of at least 15°C in which temperatures were increased to more than 50°C near the probe (Fig 3c), resulting in tissue damage confirmed by means of gross examination after MR imaging (Fig E4b [online]). Some ghosting artifacts due to motion are evident in thermometry data in regions distant to the probe (Fig 3c).

A preablation MR image with the semirigid probe in the rabbit thigh in vivo is shown in Figure E5a (online). MR thermometry maps (Fig E5b [online]) document temperatures above 85°C near the probe, which caused an ablation that was confirmed at gross examination postmortem (Fig E5c [online]). Pre- and postablation relaxometry showed T1 increases of 18% (593 msec  $\pm$  117 vs 703 msec  $\pm$  193), while T2 decreased by 8% (111 msec  $\pm$  12 vs 102 msec  $\pm$  13).

## Discussion

In this study, we demonstrated that a single loopless antenna can be configured to acquire high-spatial-resolution MR images at 3 T, locally deliver RF energy, monitor that delivery with MR thermometry, and assess the outcome of the ablation by means of relaxometry. The computations show that the loopless antenna can deliver a thermal dose commensurate with the RF input power level and duration. Tissues subject to temperatures in

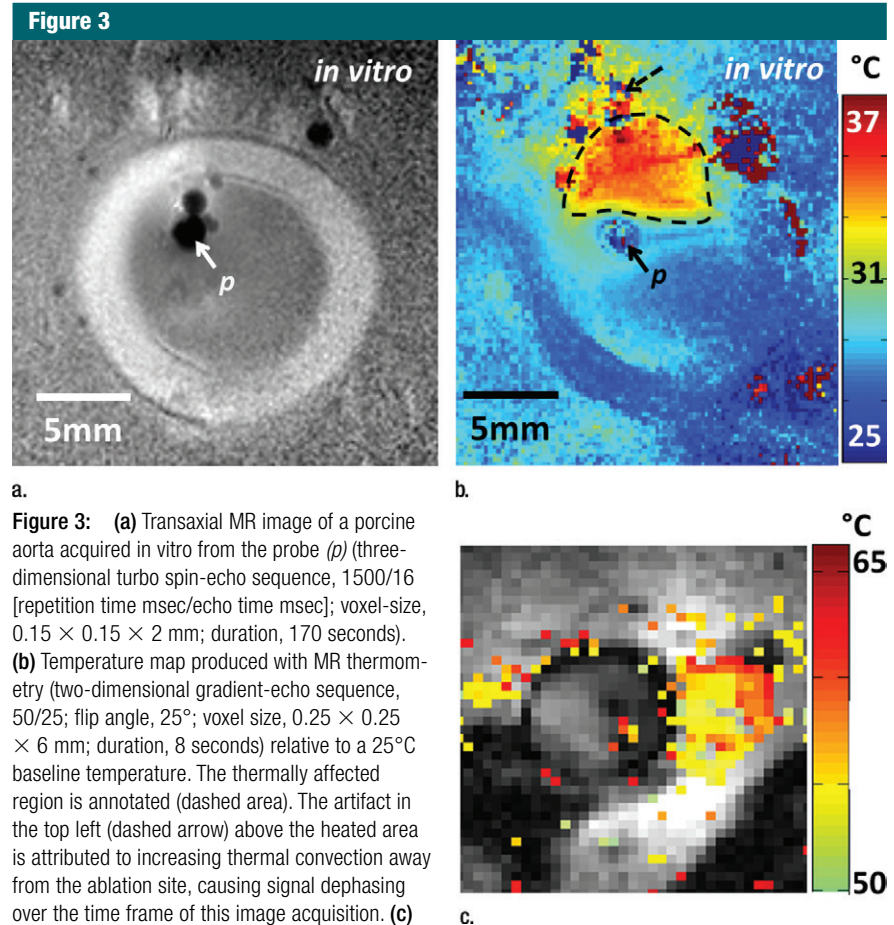


**Figure 3:** (a) Transaxial MR image of a porcine aorta acquired in vitro from the probe (p) (three-dimensional turbo spin-echo sequence, 1500/16 [repetition time msec/echo time msec]; voxel-size, 0.15  $\times$  0.15  $\times$  2 mm; duration, 170 seconds). (b) Temperature map produced with MR thermometry (two-dimensional gradient-echo sequence, 50/25; flip angle, 25°; voxel size, 0.25  $\times$  0.25  $\times$  6 mm; duration, 8 seconds) relative to a 25°C baseline temperature. The thermally affected region is annotated (dashed area). The artifact in the top left (dashed arrow) above the heated area is attributed to increasing thermal convection away from the ablation site, causing signal dephasing over the time frame of this image acquisition. (c) Temperature map acquired with MR thermometry (two-dimensional gradient-echo sequence, 41/25; flip angle, 24°; voxel size, 0.3  $\times$  0.3  $\times$  8 mm; and duration, 6 seconds) in the target area from Figure E4a (online), overlaid on the MR image.

excess of 42°C are considered thermally stressed, with temperatures above 60°C being required for tissue necrosis (18). Experimentally, we achieved temperature increases above 85°C, resulting in irreversible tissue damage, consistent with computed thermal profiles. However, the number of studies, while demonstrating the technology, is insufficient to fully evaluate ablation effectiveness. It is important to recognize that the thermal dose and the anatomic extent of the ablation will, in practice, depend on the tissue properties, including perfusion and flow. The inherent variability of this process underscores the need for a means of monitoring both the temperature increase and its ultimate effect on the surrounding tissue—in this case, using the high-spatial-resolution MR imaging

thermometry and relaxometry afforded by the ablation probe itself.

Good thermal contact between the probe and the tissue is important for effective delivery of the RF energy. Temperatures over 75°C produced a sizeable burn lesion in bovine muscle tissue and rabbit thigh where the probe was in direct contact with the tissue. However, temperature increases were smaller in porcine and rabbit aortas in vitro and in vivo. Here, the thermal dose and resultant injury were limited by thermal conduction in the fluid (saline or blood) within the vessel, as was consistent with prior observations (23). Heterogeneity on the pre- and postablation T1 and T2 maps reflects different tissue compositions (muscle, cartilage, fat, etc) (24). After ablation, increases

in T2 in vitro likely reflect the response of adipose components to the heating, while the T2 decreases seen in vivo can include the effects of hemorrhage, edema, and perfusion.

In our setup, the time to switch between RF energy delivery and MR imaging was 3–5 seconds. This delay, while small compared with the total ablation periods, may cause some underestimation of the thermal dose measured with MR imaging thermometry. By extrapolating the proton resonance frequency data, the underestimation was relatively small (temperature change < 3°C at a distance of 2 mm from the probe). Simultaneous MR imaging and RF ablation at different frequencies could eliminate such underestimation with suitable RF filtering (10). Motion artifacts that occur during parametric imaging and phase-sensitive thermal mapping sequences may be addressed by using interventional MR imaging-specific motion-correction techniques (25). The antenna design is safe for in vivo MR imaging (5), but additional anchoring in vessels may improve imaging, ablation efficiency, and accuracy. The temperature changes of more than 50°C close to the probe that confounded the proton resonance frequency algorithm may be solved by increasing the temporal resolution, albeit at a cost to spatial resolution.

In conclusion, we have shown that an MR imaging–active interventional loopless antenna at 128 MHz can be configured to receive high-spatial-resolution MR imaging signals at 3 T and locally apply RF heating to a sample. A single, minimally invasive MR imaging probe can thus be used to perform the functions of RF ablation, high-spatial-resolution imaging, and thermal monitoring of the ablation. It could thus serve as an integrated vehicle for detecting localized pathologic abnormalities and for the delivery and monitoring of therapy.

**Disclosures of Conflicts of Interest:** M.A.E. disclosed no relevant relationships. S.S.H. Activities related to the present article: disclosed no relevant relationships. Activities not related to the present article: author is currently an employee of Philips Healthcare, India. Other re-

lationships: disclosed no relevant relationships. P.A.B. disclosed no relevant relationships.

## References

- Lewin JS, Connell CF, Duerk JL, et al. Interactive MRI-guided radiofrequency interstitial thermal ablation of abdominal tumors: clinical trial for evaluation of safety and feasibility. *J Magn Reson Imaging* 1998;8(1):40–47.
- Tuncali K, Morrison PR, Zientara GP. MRI monitoring and control of cryoablation. In: Jolesz FA, ed. *Intraoperative imaging and image-guided therapy*. New York, NY: Springer, 2014; 397–401.
- Terraz S, Salomir R, Becker CD. MR-guided radiofrequency ablation of liver tumours. In: Jolesz FA, ed. *Intraoperative imaging and image-guided therapy*. New York, NY: Springer, 2014; 799–816.
- Volland NA, Kholmovski EG, Parker DL, Hadley JR. Initial feasibility testing of limited field of view magnetic resonance thermometry using a local cardiac radiofrequency coil. *Magn Reson Med* 2013;70(4):994–1004.
- El-Sharkawy AM, Qian D, Bottomley PA. The performance of interventional loopless MRI antennae at higher magnetic field strengths. *Med Phys* 2008;35(5):1995–2006.
- Sathyanarayana S, Schär M, Kraitchman DL, Bottomley PA. Towards real-time intravascular endoscopic magnetic resonance imaging. *JACC Cardiovasc Imaging* 2010;3(11):1158–1165.
- Ertürk MA, El-Sharkawy AM, Bottomley PA. Interventional loopless antenna at 7 T. *Magn Reson Med* 2012;68(3):980–988.
- Sathyanarayana S, Bottomley PA. MRI endoscopy using intrinsically localized probes. *Med Phys* 2009;36(3):908–919.
- Qiu B, Yeung CJ, Du X, Atalar E, Yang X. Development of an intravascular heating source using an MR imaging guidewire. *J Magn Reson Imaging* 2002;16(6):716–720.
- Qiu B, El-Sharkawy AM, Paliwal V, et al. Simultaneous radiofrequency (RF) heating and magnetic resonance (MR) thermal mapping using an intravascular MR imaging/RF heating system. *Magn Reson Med* 2005;54(1):226–230.
- Ocali O, Atalar E. Intravascular magnetic resonance imaging using a loopless catheter antenna. *Magn Reson Med* 1997;37(1):112–118.
- Ghugre NR, Ramanan V, Pop M, et al. Quantitative tracking of edema, hemorrhage, and microvascular obstruction in subacute myocardial infarction in a porcine model by MRI. *Magn Reson Med* 2011;66(4):1129–1141.
- Verhaert D, Thavendiranathan P, Giri S, et al. Direct T2 quantification of myocardial edema in acute ischemic injury. *JACC Cardiovasc Imaging* 2011;4(3):269–278.
- Ding H, Fernandez-de-Manuel L, Schär M, et al. Three-dimensional whole-heart T2 mapping at 3T. *Magn Reson Med* 2015;74(3):803–816.
- Moros E. *Physics of thermal therapy: fundamentals and clinical applications*. Boca Raton, Fla: Taylor & Francis, 2012.
- Yarmolenko PS, Moon EJ, Landon C, et al. Thresholds for thermal damage to normal tissues: an update. *Int J Hyperthermia* 2011;27(4):320–343.
- Graham SJ, Chen L, Leitch M, et al. Quantifying tissue damage due to focused ultrasound heating observed by MRI. *Magn Reson Med* 1999;41(2):321–328.
- Chang IA. Considerations for thermal injury analysis for RF ablation devices. *Open Biomed Eng J* 2010;4:3–12.
- In den Kleef JJ, Cuppen JJ. RLSQ: T1, T2, and  $\rho$  calculations, combining ratios and least squares. *Magn Reson Med* 1987;5(6):513–524.
- Ishihara Y, Calderon A, Watanabe H, et al. A precise and fast temperature mapping using water proton chemical shift. *Magn Reson Med* 1995;34(6):814–823.
- Ertürk MA, El-Sharkawy AM, Bottomley PA. Monitoring local heating around an interventional MRI antenna with RF radiometry. *Med Phys* 2015;42(3):1411–1423.
- El-Sharkawy AM, Qian D, Bottomley PA, Edelstein WA. A multichannel, real-time MRI RF power monitor for independent SAR determination. *Med Phys* 2012;39(5):2334–2341.
- Goldberg SN, Gazelle GS, Halpern EF, Ritman WJ, Mueller PR, Rosenthal DI. Radiofrequency tissue ablation: importance of local temperature along the electrode tip exposure in determining lesion shape and size. *Acad Radiol* 1996;3(3):212–218.
- Gold GE, Han E, Stainsby J, Wright G, Brittain J, Beaulieu C. Musculoskeletal MRI at 3.0 T: relaxation times and image contrast. *AJR Am J Roentgenol* 2004;183(2):343–351.
- Hegde SS, Zhang Y, Bottomley PA. Acceleration and motion-correction techniques for high-resolution intravascular MRI. *Magn Reson Med* 2015;74(2):452–461.